Thermal and Quenched Fluctuations of Polymer Concentration in Poly(dimethylsiloxane) Gels

Catherine Rouf-George,[‡,||] Jean-Pierre Munch,[*,†] François Schosseler,[†] Alain Pouchelon,[||] Gérard Beinert,[‡] François Boué,[§] and Jacques Bastide[‡,⊥]

Laboratoire de Dynamique des Fluides Complexes, Université Louis Pasteur, 4 rue Blaise Pascal, 67070 Strasbourg Cedex, France, Institut Charles Sadron, 6 rue Boussingault, 67083 Strasbourg Cedex, France, Laboratoire Léon Brillouin, Laboratoire commun CEA-CNRS, CEN Saclay, 91191 Gif sur Yvette Cedex, France, and Rhône-Poulenc Silicones, 55, Avenue des Frères Perret, BP 22, 69191 Saint-Fons Cedex, France

Received June 24, 1997; Revised Manuscript Received September 23, 1997[⊗]

ABSTRACT: Using neutron and light scattering techniques, we studied, as a function of swelling degree in a good solvent, the fluctuations of polymer concentration in highly cross-linked gels prepared in the bulk. Using the method proposed by Pusey and Van Megen, we separated the total scattering intensity into the contributions arising from thermal and quenched fluctuations. The former are equivalent to those measured in an entangled polymer solution with same concentration while the latter are responsible for the excess of intensity scattered from swollen gels and for the typical anisotropic intensity patterns measured on elongated gels. The relaxation of the thermal fluctuations is still governed by the cooperative diffusion of all the chains in the gel, and the associated characteristic length is the screening length for excluded and hydrodynamic interactions. We propose a new picture for fluctuations of concentration in polymer gels and discuss it in relation with recent models.

I. Introduction

Polymer gels are very unique systems because they exhibit liquidlike behavior on microscopic length scales and solidlike properties at the macroscopic level.[1−5] The transition between these two characteristic behaviors occurs because at some intermediate length scale permanent topological constraints are exerted due to the existence of cross-links and of excluded volume interactions. These topological constraints are randomly distributed in the medium due to the fluctuations in the functionality of the cross-links, the fluctuations in the chain length between topologically adjacent cross-links and the influence of entanglements. Thus the phenomenon at the origin of the unique properties of gels is associated with quenched disorder, the characterization of which is a challenging task.

This is partly due to the fact that our main tools of investigation, like radiation scattering[6,7] or permeation[8] experiments, are indirect ones and probe the fluctuations of concentration in the medium. As a result of quenched topological constraints, the fluctuations of concentration comprise both thermal and quenched components. The thermal part reflects the liquidlike aspect of the gel and includes the dynamic spatial fluctuations of concentration that are constantly rebuilt through the Brownian motion of the scatterers. Conversely, the quenched part corresponds to a spectrum of spatial fluctuations that are frozen-in by the quenched topological constraints. Both types of fluctuations contribute to the intensity measured in a radiation scattering experiment, and therefore, it is necessary to distinguish them in order to characterize the quenched disorder associated to the topological constraints, which is revealed essentially by the quenched fluctuations of concentration.

This problem is the main concern of the present paper and can be solved by using the scanning light scattering method proposed by Pusey and Van Megen[9] for the study of systems containing Brownian scatterers with limited excursion around fixed average positions. Later this method has been used to study polymer gels[10−15] with, however, varying interpretations for the origin of the large intensity fluctuations that are measured while scanning through different scattering volumes of a sample. These divergences result partly from the fact that most of the previously published works deal with lightly cross-linked gels studied in their reaction bath, which means that the frozen scattering intensity remains a small fraction of the total scattering intensity. In the present work, we study poly(dimethylsiloxane) gels prepared in the melt as a function of swelling degree. Due to their high cross-linking density, their equilibrium swelling degree is about 6 and the ratio of the quenched intensity to the fluctuating intensity can be as high as about 15. This allows us to resolve the above mentioned divergences.

The paper is organized as follows. In section II, we introduce the notations and give the principles of the method. Section III details the experimental procedures. The results of small angle neutron scattering and of static and dynamic light scattering experiments are described in section IV and discussed in section V.

II. Theoretical Background

The structure of gels and solutions can be conveniently studied by means of radiation scattering techniques.[6] Incident quantum particles (neutrons or photons) interact with the constituents of the sample and a finite fraction of them is scattered isotropically. Due to the wavelike nature of the particles, the scattering intensity reflects the interference pattern arising from the phase shifts associated with their optical paths and thus characterizes the spatial organization of the con-

[†] Université Louis Pasteur.
[‡] Institut Charles Sadron.
[§] CEN Saclay.
[||] Rhône-Poulenc Silicones.
[⊥] Deceased.
[⊗] Abstract published in *Advance ACS Abstracts,* December 1, 1997.

S0024-9297(97)00916-9 CCC: $14.00 © 1997 American Chemical Society

stituents in the sample. Because of the presence of the cross-links, gels are actually ternary mixtures. However, since the volume fraction of the cross-links is very low and since their structure is very close to that of the polymer chains (the larger ones are made of siloxane tetramers), it is not necessary to take into account explicitly this third component.[16] Therefore the solutions or the gels we studied can be considered as binary mixtures containing monomers and solvent molecules. As a result, the instantaneous scattering intensity, $I(\mathbf{q},t)$, measured at time t in a point located at infinite distance from the sample (far detection limit) can be written as

$$I(\mathbf{q},t) \propto \int_V\int_{V'}\Delta\phi(\mathbf{r},t)\,\Delta\phi(\mathbf{r}',t)\mathrm{e}^{-i\mathbf{q}(\mathbf{r}-\mathbf{r}')}\,\mathrm{d}^3\mathbf{r}\,\mathrm{d}^3\mathbf{r}' \quad (1)$$

Here $\mathbf{q}$ is the scattering vector $\mathbf{q} = \mathbf{k}_\mathrm{i} - \mathbf{k}_\mathrm{s}$, $\mathbf{k}_\mathrm{i}$ and $\mathbf{k}_\mathrm{s}$ denoting respectively the wavevectors of the incident and of the scattered particles. In the approximation of elastic scattering, $k_\mathrm{i} = k_\mathrm{s} = 2\pi/\lambda$ and $q = (4\pi/\lambda)\sin(\theta/2)$, where θ denotes the scattering angle, i.e. the angle between $\mathbf{k}_\mathrm{i}$ and $\mathbf{k}_\mathrm{s}$. In the far detection limit the scattering angle can be considered to be the same for all the scattered particles and the vector $\mathbf{q}$ is uniquely defined. In eq 1, the integration is performed over the scattering volume $V = V'$ and $\Delta\phi(\mathbf{r},t)$ represents the local fluctuation of polymer concentration defined as

$$\Delta\phi(\mathbf{r},t) \equiv \phi(\mathbf{r},t) - \phi \quad (2)$$

where $\phi(\mathbf{r},t)$ and ϕ denote the local instantaneous polymer concentration at point $\mathbf{r}$ and the average macroscopic concentration in the system, respectively. In the following, we consider only the case of small but still macroscopic scattering volumes which means that, at any time, we have the condition

$$\int_V\Delta\phi(\mathbf{r},t)\,\mathrm{d}^3\mathbf{r} = 0 \quad (3)$$

Equation 3 simply states that the average number of scattering units in the volume V can be considered as a constant. For systems with partly frozen-in fluctuations of concentration we can split $\Delta\phi(\mathbf{r},t)$ as

$$\Delta\phi(\mathbf{r},t) \equiv \delta\phi_\mathrm{c}(\mathbf{r}) + \delta\phi_\mathrm{f}(\mathbf{r},t) \quad (4)$$

where $\delta\phi_\mathrm{c}(\mathbf{r})$ represents the time average deviation of the local concentration with respect to ϕ and $\delta\phi_\mathrm{f}(\mathbf{r},t)$ denotes the instantaneous deviation with respect to $\delta\phi_\mathrm{c}(\mathbf{r})$ at time t. Thus $\delta\phi_\mathrm{f}(\mathbf{r},t)$ has a zero mean value

$$\langle\delta\phi_\mathrm{f}(\mathbf{r},t)\rangle_T = 0 \quad (5)$$

where the brackets $\langle\ \rangle_T$ represent a time-averaged value.

Equations 1−5 are the basis to understand the output of a practical intensity measurement that involves always different kinds of averaging processes.[9] The first one is a time average performed during the time interval T that is necessary to complete the measurement. Its effect depends on the ratio of T to the characteristic time T_c of thermal fluctuations in the system. For large values of this ratio, the time-averaged intensity is, within the statistical errors, a constant equal to $I(\mathbf{q}) = \langle I(\mathbf{q},t)\rangle_T$. For small values of the ratio T/T_c, the time-averaged intensity can be considered to be equal to its instantaneous value and a large set of different measurements will be described by a density of probability $P(I(\mathbf{q},t))$. In the case of random fluctuations, one gets the classical result[9,17−19]

$$P(I(\mathbf{q},t)) = \frac{1}{I(\mathbf{q})}\exp\left\{-\frac{I(\mathbf{q},t)}{I(\mathbf{q})}\right\} \quad (6)$$

A second type of average is spatial and is introduced by the finite area of the detector, the finite size of the scattering volume, and the finite distance between sample and detector.[20] If we consider two points M and P separated by a distance d on the surface of the detector, there is a difference in the scattered wavevector of the waves detected in M and P and thus a difference in their phase. When this phase difference becomes larger than about 2π, the amplitudes of the two scattered waves are no longer correlated. A similar argument can be developed if we consider the detection, on one point of the detector, of the intensity scattered from a finite volume of the sample with a characteristic size L perpendicular to the incident wave. In both cases, for sufficiently large d or L values, the time average involved in the measurement is performed incoherently on a set of uncorrelated scattered waves. These arguments define the coherence area that is a measure of the surface of the detector (or equivalently of the scattering volume) over which the temporal fluctuations of the scattered waves remain correlated. More quantitatively, the number of coherence areas n involved in a given scattering geometry can be defined as $n \approx S\Omega/\lambda^2$ where S is the area of detection and Ω the solid angle spanned by this area as seen from one point in the scattering volume. Alternately, S can be considered as the surface of the scattering volume and Ω the solid angle spanned by that surface as seen from one point of the detector. One consequence is that the effort to reach low n values has to be put on both the size of the scattering volume and the surface area of the detector. As n becomes larger than unity, the decorrelation effects have the consequence that the measured scattering intensity is the average of the coherent time-averaged intensities from each coherence area. Accordingly, the distribution of intensities $P(I(\mathbf{q},t))$ is modified, and for the case of random fluctuations, in the limit $T \ll T_\mathrm{c}$, it reads[20,21]

$$P(I(\mathbf{q},t)) = \frac{1}{\Gamma(n)}\left(\frac{n}{I(\mathbf{q})}\right)^n (I(\mathbf{q},t))^{n-1}\exp\left(-\frac{nI(\mathbf{q},t)}{I(\mathbf{q})}\right) \quad (7)$$

where $\Gamma(n)$ is Euler's gamma function. As n increases, the distribution of intensities becomes more and more sharply peaked around its mean value $I(\mathbf{q})$. Thus long time averaging ($T \gg T_\mathrm{c}$) and extended spatial integration result in the same value for the measured intensity in the case of random fluctuations.

In the case of frozen fluctuations of concentration, we are formally in the limit $T \ll T_\mathrm{c}$ whatever the duration of the measurement. Thus for randomly distributed frozen fluctuations, in the case of a detection on one coherence area, one could probe forever one realization of the possible intensity values described by the distribution in eq 6. This realization corresponds to one given set of random phases in eq 1. Then the only possibility for reaching a meaningful average value is to randomize the realization of these phases.[9,22,23] In practice this can be done by increasing n, by averaging the speckle pattern on the detector, by rotating the sample, or by averaging a large set of measurements performed on different scattering volumes. The last procedure is called an ensemble average and is noted $\langle\ \rangle_\mathrm{E}$ in the following.

An interesting situation is one where the fluctuations of concentration are partly quenched (eq 4) and where the time average is performed on a duration that is large compared to the characteristic time of the thermal fluctuations ($T \gg T_c$). Both the thermal and the quenched fluctuations of concentration contribute to the scattering intensity. Inserting (4) into (1), performing the time average and taking into account (5), one is left with[9]

$$I_i(\mathbf{q}) = I_{c,i}(\mathbf{q}) + I_f(\mathbf{q}) \tag{8}$$

where the index i labels the scattering volume V_i and

$$I_{c,i}(\mathbf{q}) \propto \int_{V_i}\int_{V_{i'}} \delta\phi_c(\mathbf{r})\, \delta\phi_c(\mathbf{r}')\, e^{-i\mathbf{q}(\mathbf{r}-\mathbf{r}')}\, d^3\mathbf{r}\, d^3\mathbf{r}' \tag{9a}$$

$$I_f(\mathbf{q}) \propto \int_V\int_{V'} \langle \delta\phi_f(\mathbf{r},t)\, \delta\phi_f(\mathbf{r}',t)\rangle_T\, e^{-i\mathbf{q}(\mathbf{r}-\mathbf{r}')}\, d^3\mathbf{r}\, d^3\mathbf{r}' \tag{9b}$$

Note that we dropped in eqs 1 and 9 the same numerical factors that are irrelevant for the present discussion. By definition, $I_f(\mathbf{q})$ is independent of the scattering volume while $I_{c,i}(\mathbf{q})$ is expected to show a strong dependence on the position in the sample. In fact, in the case of a detection on one coherence area, the distribution of the values for $I_{c,i}(\mathbf{q})$ is expected to obey eq 6 with $I(\mathbf{q},t)$ replaced by $I_{c,i}(\mathbf{q})$. As a consequence the distribution of the measured intensities $I_i(\mathbf{q})$ while exploring different scattering volumes is shifted and is given by[10]

$$P(I_i(\mathbf{q})) = \frac{H[I_i(\mathbf{q}) - I_f(\mathbf{q})]}{\langle I_i(\mathbf{q})\rangle_E - I_f(\mathbf{q})} \exp\left[-\frac{I_i(\mathbf{q}) - I_f(\mathbf{q})}{\langle I_i(\mathbf{q})\rangle_E - I_f(\mathbf{q})}\right] \tag{10}$$

where $H(x)$ is the Heaviside step function. Thus, the existence of a fluctuating intensity implies that no completely destructive interference (dark speckle) can exist anymore if the duration of the experiment is long enough ($T \gg T_c$) and that intensities values smaller than a typical threshold, related to the thermal fluctuations, are now forbidden.

It can be noted that, in a neutron scattering experiment, due to the incoherence of the incident beam, to the duration of the experiment and to the size of the scattering volume, one measures always the ensemble averaged value $\langle I_i(\mathbf{q})\rangle_E$ of the distribution in eq 10. For the sake of simplicity, this value will often be noted in the following, when no ambiguity is possible, as $I_E(\mathbf{q})$ or even as $I(\mathbf{q})$ (in the case of neutron scattering experiments). From eq 8, it follows directly that[9]

$$I_E(\mathbf{q}) = I_c(\mathbf{q}) + I_f(\mathbf{q}) \tag{11}$$

where $I_c(\mathbf{q}) \equiv \langle I_{c,i}(\mathbf{q})\rangle_E$.

We now turn to quasi-elastic light scattering experiments. The measured quantity is the normalized intensity correlation function (ICF)

$$g_i^{(2)}(\mathbf{q},t) = \frac{\langle I_i(\mathbf{q},t')I_i(\mathbf{q},t'+t)\rangle_T}{I_i^{\,2}(\mathbf{q})} \tag{12}$$

where $I_i(\mathbf{q},t)$ is given by eq 1 and we use the index i as before to specify the scattering volume. Using eqs 1−5 and performing the time average as before, we obtain[9,24]

$$g_i^{(2)}(\mathbf{q},t) = 1 + \frac{2I_f(\mathbf{q})I_{c,i}(\mathbf{q})}{I_i^{\,2}(\mathbf{q})} g_f^{(1)}(\mathbf{q},t) + \frac{I_f^{\,2}(\mathbf{q})}{I_i^{\,2}(\mathbf{q})}[g_f^{(1)}(\mathbf{q},t)]^2 \tag{13}$$

where $g_f^{(1)}(\mathbf{q},t)$ is the normalized self-correlation function of the fluctuating electric field

$$g_f^{(1)}(\mathbf{q},t) = \frac{\langle E_f(\mathbf{q},t')E_f^*(\mathbf{q},t'+t)\rangle_T}{I_f(\mathbf{q})} \tag{14}$$

and the scattered field is proportional to the Fourier transform of the thermal fluctuations of concentration

$$E_f(\mathbf{q},t) \propto \int_V \delta\phi_f(\mathbf{r},t) e^{-i\mathbf{q}\mathbf{r}}\, d^3\mathbf{r} \tag{15}$$

It can be noticed that, in writing eq 14, we assume implicitly that the time correlation of the fluctuating intensity is independent of the scattering volume, which goes one step further than stating that its time average does not depend on the scattering volume. We can define an ensemble averaged ICF over p scattering volumes as[9]

$$g_E^{(2)}(\mathbf{q},t) = \frac{\frac{1}{p}\sum_{i=1}^{p} I_i^{\,2}(\mathbf{q}) g_i^{(2)}(\mathbf{q},t)}{I_E^{\,2}(\mathbf{q})} \tag{16}$$

In the case of a medium with partly quenched fluctuations of concentration, this quantity exhibits statistical properties that are different from that of the ICF measured from one scattering volume (eq 12), as was shown in detail in refs 9 and 10. In particular, the long time tail of the ensemble averaged ICF does not decay to 1. Equation 16 can be used to define the ensemble averaged dynamic structure factor $f_E(\mathbf{q},t)$ through Siegert's relationship[25]

$$f_E(\mathbf{q},t) = [g_E^{(2)}(\mathbf{q},t) - 1]^{1/2} \tag{17}$$

provided that the detection is performed on one single coherence area and that the scattering from the solvent can be neglected. In practice the contribution of the solvent, although very small, is not always negligible and can be taken into account in a way that is summarized in the Appendix.

III. Experimental Section

1. Sample Preparation. In this paper, we studied a set of PDMS solutions and four PDMS networks. The solutions were prepared from two industrial polymers (Rhône-Poulenc), a "gum" and an "oil" with average molecular weight (M_n) equal to 2.5×10^5 and 7.2×10^4, respectively. The distribution of molecular weights are rather large in both cases (M_w/M_n = 2−3). Before use the "gum" was dissolved in cyclohexane and precipitated in methanol, in order to remove impurities and low molecular weight species, such as, e.g., unreacted cyclic tetramers. Size exclusion chromatography with toluene as eluent was used to characterize the precipitate and yielded $M_n = 2.7 \times 10^5$ and $M_w/M_n = 3.0$. For all light scattering studies and for some of the neutron ones, the solutions were filtered using a 0.45 μm filter.

Three different methods, all performed in bulk, were used to prepare the networks. The first method may be called a "vulcanization" process, since, under the action of γ-irradiation (^{60}Co source), tie-points are established at random in between the chains of the "gum" mentioned above. Samples were molded by spreading the reprecipitated gum in between two

Table 1. Summary of the Sample Features[a]

sample	synthesis	Q_{max}	G_{bulk} (10^3 Pa)	sol fraction (%)
γ_A	γ irradiation 24150 Gy	6.5	120	6.3
γ_B	γ irradiation 53870 Gy	6	160	5.6
9800SiVi	end-linking	6.5	160	7.3
9200SiH	end-linking	6.3 ± 0.25	100	9.6

[a] Q_{max} = volume of the gel immersed in a solvent bath/volume of the unswollen network. G_{bulk} = elastic modulus (see text) of the unswollen network, after extraction of the soluble fraction.

microcope glass slides separated by a rubber joint about 1 mm thick, cut in a Viton foil. Metal clamps were used to press the glass slides against the joint. No bubble were left in these molds but the polymer had not been degassed. The polymer chains of the "gum" carry side chain vinyl groups (720 ppm) which presumably contribute to the cross-linking reaction. Surprisingly enough, they also prevent the chemical grafting of the PDMS rubber onto the glass slides that has been observed in the case of chains without vinyl side groups. For the present study, two samples were obtained using this method. They differ by the duration of the imposed γ-irradiation, namely 13 days for sample γ_A and 29 days for sample γ_B (see Table 1).

The two other methods of network formation involve the end-linking of much shorter chains ($M_n \approx 10^4$) with tetrafunctional molecules. In both cases, the cross-linking is performed through an hydrosilylation reaction occurring between SiH and $SiCH{=}CH_2$ (SiVi) groups, in the presence of a platinum catalyst.

Along end-linking method A, vinyl terminations of the chains ($M_n \approx 9800$, $M_w/M_n \approx 2$) react with four SiH groups carried by cyclic siloxane tetramers (D′4). The components, in stoichiometric ratio, were mixed with 10 ppm of Karstedt catalyst,[26] and the mixture was poured into an aluminium mold on which Duponol had been spread in order to prevent adhesion between the rubber and the metal. The cross-linking reaction starts at room temperature but in order to complete it, the filled mold was put into an oven at 70 °C during 48 h.

Cross-linking method B is the complement of the preceding one: the SiH groups are carried by the chain extremities whereas the cross-linking molecules consist of cyclic tetramers with four vinyl side groups. The precursor chains are very comparable to those of the previous synthesis: $M_n = 9200$, $M_w/M_n \approx 2.2$. In the present case, the catalyst is chloroplatinic acid,[27] which allows a slower reaction than the Karstedt catalyst. Thus it allowed the filtration of the mixture precursor chains + cross-linker + catalyst through a 0.45 μm filter while filling the molds. Such networks were indeed devoted to light scattering experiments, for which it is critical to remove dust particles from the samples. These were made in the form of either cylinders or parallelepipeds. The cylindrical samples were prepared by casting the pregel mixture in polypropylene tubes engaged in air tight glass tubes. To study the kinetics of swelling, one cylindrical sample with small diameter (28 mm) was also prepared in a polyethylene pipe of about 15 cm length. Sheets of rubber were obtained with a mold made of polypropylene walls maintained by aluminium holders and tightened by bolts and nuts. The thickness of the sample could be tuned by varying the thickness of teflon cross-pieces, inserted between the walls of the mold. To prevent adhesion, these walls were covered with a thin layer of polyethylene terephtalate. The cross-linking reaction was completed upon heating in an oven at 70 °C over 48 h. As noted above, this cross-linking reaction does not start in a detectable manner at room temperature, and as will be shown below, it is also less complete.

All the prepared network samples were thoroughly washed in cyclohexane, for at least 2 weeks. The solvent was replaced at least 10 times and the sol fraction was measured (see Table 1). After washing, the solvent was replaced by toluene, which in turn was slowly evaporated. Then the samples were dried under vacuum in an oven, until a constant weight was reached.

The states of incomplete swelling which have been studied were attained with a good precision by weighing. For instance, disks of dry PDMS rubber were put in the neutron scattering cells (two disks of quartz tightened by an aluminium sample holder on a glass circular ring with parallel faces) in which one weighed the required amount of deuterated toluene for reaching a given swelling degree Q. After typically 2 days, the set formed by the sample, the cell, and the cell holder was weighed again, and if necessary, the amount of solvent was corrected for after reopening of the cell. In such a situation, the precision on the swelling degree Q is about $\pm 1\%$ or even less. For isotropic light scattering experiments, we used cylindrical samples, which we let swell in cylindrical tubes made of optical glass on which an airtight cork had been sealed. The swelling degree at which we studied the samples were dictated by the ratio of the bores of the glass tubes (which was varied) over the diameter of the dry samples. In a first step, we put the dry samples in the tubes and we added a little less than the required amount of solvent for reaching the calculated swelling ratio. After complete absorption of the solvent by the sample, we added progressively the remaining part of the solvent in order to achieve a thorough optical contact between the gel and the glass.

We considered also a situation of anisotropic swelling, which was achieved owing to a method analogous to the one developped in a slightly different context by Geissler et al.:[28] an ellipse with major and minor axes respectively equal to 20 and 10 mm was cut in a sheet of filtered rubber 9200SiH of thickness equal to 3.6 mm. This elliptical piece of rubber was put in a cell having the shape of a disk (diameter, 25mm; thickness, 4.62 mm) which was filled with toluene. The sample absorbed the solvent and was forced by the walls of the cell to swell anisotropically. As a result, in the final state, this PDMS gel is submitted to anisotropic deformation ratios with respect to the dry state: $\alpha_m = 2.5$, $\alpha_M = 1.25$, and $\alpha_{th} = 1.25$ along the minor axis, the major axis, and the thickness, respectively. As a whole the swelling degree is $Q = 3.9$, which would correspond, if the swelling was isotropic, to a deformation in every direction of $\alpha_{av} = 1.57$. Therefore, the gel is extended along the direction of the minor axis, by a factor $\Lambda = \alpha_m/\alpha_{av} = 1.59$, whereas it is compressed along the two perpendicular directions (those of the major axis and of the thickness) by a factor $\Lambda' = \alpha_M/\alpha_{av} = 0.80 \approx (1.58)^{-1/2}$. As a result, everything happens as if the gel was uniaxially extended by a factor 1.58 with respect to an isotropically swollen state such as $Q = 3.9$. A part of the results regarding anisotropically swollen gels has already been published.[14]

2. Sample Characterization. Mechanical Properties. The mechanical properties of the dry netwoks were characterized by using a homemade stretching machine. The samples (about $7 \times 1.5 \times 0.1$ cm) were fixed by self-tightening clamps to jaws driven by a stepping motor and controlled by a desktop computer. The separation of the jaws was measured by a ruler with optical encoding read by the computer, from which the stretching ratio $\alpha = L/L_0$ between clamps was calculated (L_0 and L denoting respectively the length of the sample, in between clamps, before and after the uniaxial deformation is imposed). A more local estimate of the stretching ratio was performed with the help of a linear CCD camera, by measuring the separation between two ink lines drawn on the samples. The lines were drawn by application of a rubber stamp, whose ink was found suitable for marking PDMS rubber. In most cases, the only ones which we kept for further examination, we observed a good agreement between the extension ratios given by the camera and by the distance between the jaws. The standard theories of rubber elasticity[1,3,29] predict the following dependence, with extension ratio, of the nominal stress:

$$\sigma_0 = A\nu^* kT(\alpha - \alpha^{-2}) \tag{18}$$

The nominal stress σ_0 represents the elastic force divided by the area of the undeformed sample in the direction perpendicular to the elongation. A is a dimensionless constant, generally assumed to range in between $^1/_2$ and 1, and ν^* denotes the number of elastically effective elementary chains per unit volume.

If the variation of σ_0 with α given by eq 18 is satisfied, one may introduce a "neo-Hookian" modulus G, defined as

$$G = \frac{\sigma_0}{(\alpha - \alpha^{-2})} \tag{19}$$

However, the mechanical data relative to unswollen networks can scarcely be fitted with a good agreement to eq 18. Therefore the determination of the modulus G of a dense rubber is often problematic. One possibility is to use the phenomenological equation of Mooney and Rivlin which reads[3,29]

$$\sigma_0 = 2C_1(\alpha - \alpha^{-2}) + \frac{C_2}{\alpha}(\alpha - \alpha^{-2}) \tag{20}$$

Equation 20 has been obtained as a first order development of equations provided by continuum mechanics. The relation of the constants C_1 and C_2 with the molecular quantities such as the density of elastically effective chemical "meshes" or the density of "trapped entanglements" is still a matter for debate. Contrary to the usual behavior for dense rubbers, eq 20 did not provide a much better description of the data for the present PDMS networks, and in the so-called Mooney−Rivlin plot, i.e., $\sigma_0/(\alpha - \alpha^{-2})$ vs $1/\alpha$, the experimental curves exhibit a downward curvature and tend toward a horizontal plateau for $\alpha \approx 1$. We chose the height of this plateau for the values given in Table 1, and this method is equivalent to the use of the result of a fit by eq 18 for α tending toward 1.

Swelling Ratio. The maximum swelling ratios Q_{max} of the different samples in toluene were measured by an optical method using a profile projector (Nikon 6C). The samples had in general the shape of disks and we measured the relative change of the diameters in between the dry state and the swollen state, the samples being immersed in a large excess of solvent. The maximum swelling ratios were calculated as $Q_{max} = (D_{max}/D_{dry})^3$, where D_{max} and D_{dry} stand for the diameters in the swollen and dry states, respectively. The precision of the measurement (±7%) is not extremely good because of the presence of irregularities on the edges of the samples, the effect of which being amplified by taking the cube of D_{max}/D_{dry} for getting Q_{max}. Nevertheless the precision is in general better than the one obtained by a weighing method, in which one has to extract from a solvent bath a sample on which an excess of solvent may remain (in the form of a superficial layer), or, on the contrary, which may lose too much solvent by evaporation.

Kinetics of Swelling. Kinetics of swelling experiments allow one to measure a macroscopic cooperative diffusion coefficient[30,31] that can be compared to the value measured by quasi-elastic light scattering experiments. The preparation of the sample has been described above. The dry sample has been transferred in an excess of toluene and the diameter of the gel cylinder has been measured as a function of time t on the screen of a profile projector by using a calibrated scale. In practice, an instability, characterized by a wrinkled surface of the gel, was observed in the early stages of the swelling, probably due to the fact that we started the experiment from the dry state. In such a case, the concentration profile within the gel is strongly deformed and the theory is not well suited to describe the early steps of the swelling. Therefore the time origin has been taken as the instant where the gel surface appears homogeneous, which is about 740 s after the gel has been put into the excess solvent. Due to the heat generated by the lamp of the profile projector, the equilibrium temperature during the experiment was about $T = 308 \pm 2$ K.

Data analysis was performed according to the theory developped by Li and Tanaka.[31] At large times t, the gel diameter $d(t)$ approaches exponentially its equilibrium value according to

$$\frac{d_f - d(t)}{d_f - d_i} = B \exp\left(-\frac{t}{\tau_1}\right) \tag{21}$$

where d_i and d_f stand for the initial and final values of the diameter, respectively. The parameter B depends only on the geometry of the gel and on the ratio ζ of the shear modulus to the longitudinal osmotic modulus. Since the dependence of B on ζ has been established numerically, the latter value can be obtained from the intercept at $t = 0$ if the data, arranged as in eq 21, are plotted on semilogarithmic scales (Figure 1). The inverse of the slope of the straight line gives the relaxation time τ_1 that allows one to calculate D_e as[31]

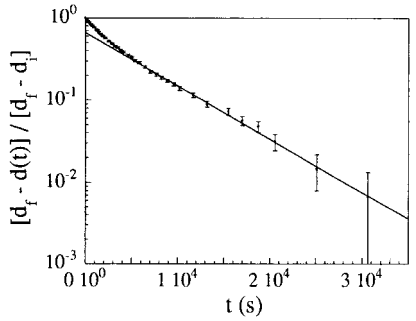

Figure 1. Evolution of the diameter of gel 9200SiH as a function of time in a kinetics of swelling experiment. The data are plotted as suggested by eq 21.

$$D_e = \frac{3}{8}\left(\frac{d_f}{X_1}\right)^2 \frac{1}{\tau_1} \tag{22}$$

where X_1 is a known function of ζ. It can be noted that, due to the mentioned instability, the first data points analyzed in this experiment have not been obtained strictly under the conditions assumed by the theory, i.e., following an osmotic shock at $t = 0$. Therefore our value for B is probably slightly changed. However, in the final steps the slope is not affected by this change in the initial conditions and it is still possible to calculate D_e values since the parameter X_1 exhibits only a small variation with B for gels with ζ values below 0.4. The analysis of the data yields the following results: $Q \approx 5.9$, $\tau_1 \approx 6800$ s, $B \approx 0.65$, $\zeta \approx 0.16$, $X_1 \approx 2.6$, and $D_e \approx 2.2 \times 10^{-6}$ cm^2 s^{-1}. We have estimated the influence of the error on B by calculating D_e with the values $B = 0.6$ and $B = 0.7$. We found $D_e \approx 2.04 \times 10^{-6}$ cm^2 s^{-1} and $D_e \approx 2.4 \times 10^{-6}$ cm^2 s^{-1}, respectively.

3. Scattering Experiments. Neutron Scattering. Neutron scattering experiments were performed at Laboratoire Léon Brillouin, Saclay (CEA-CNRS), France, on spectrometers PAXY and PACE, and at Institut Laue Langevin, Grenoble, France, on spectrometer D11. Various combinations of sample−detector distances and wavelengths λ have been tried in order to cover a q range as large as possible (they are indicated in the figure captions). To vary the q range one can act on either the wavelength λ or the sample−detector distance D_{sd}. To reach small q values, raising the wavelength is the less expensive solution in terms of neutron flux but leads frequently to slight discrepancies when trying to superpose spectra obtained this way at very small q values ($q < 10^{-2}$ Å^{-1}) and those obtained in the standard q range ($q > 10^{-2}$ Å^{-1}). As a matter of fact, differences of about 10−15% are sometimes observed even after suitable normalization. When such problems occurred, the spectrum corresponding to the larger q values was chosen as a reference. We checked indeed that spectra obtained for $D_{sd} = 4-5$ m and $\lambda = 8-10$ Å on the different spectrometers superposed nicely after conventional data treatment (see below). When we could enlarge the q range by acting only on the sample−detector distance, the superposition of the spectra was very satisfactory.

All the neutron scattering experiments reported in this paper have been performed on networks swollen by deuterated toluene or on solutions made with this solvent. Conventional data treatment was applied to the results. After correction for electronic noise, the measured neutron intensities were divided by incident intensities and by transmission. Then the signal of an empty cell, corrected and normalized the same way, was subtracted, and the result was divided by the sample thickness. Corrections for detector efficiency and conversion

to absolute units (cm^{-1}) are made by normalizing the obtained spectrum with a spectrum of water, corrected as described above for electronic noise, incident flux, transmission, and thickness, and by multiplying the result by the differential incoherent cross-section, per unit volume, of water, $d\Sigma/d\Omega$, whose values can be found in Ragnetti et al.[32] The spectrum corrected and normalized this way, $I_t(q)$, is a sum of the coherent cross-section per unit volume, $I(q)$, which is q-dependent and contains the structural information about the sample, and of the incoherent scattering cross section per unit volume, $I_{inc}(\phi)$, which is q-independent and remains to be subtracted.

For each polymer volume fraction, $I_{inc}(\phi)$ can be estimated by a linear interpolation method. We measured independently the scattering from deuterated toluene and from a PDMS melt. We checked that the scattering by a melt is identical to that of a piece of unswollen network, but we routinely choose the scattering from the melt because the precision on the thickness is better: it is that of the container, the quartz cell (about 0.1%). Following the correction and normalization procedure leading to $I_t(q)$, we obtained $I_{Dtol}(q)$ and $I_{PDMS}(q)$, for deuterated toluene and PDMS, respectively. These spectra appeared to be q-independent, which was expected since they originate almost entirely from incoherent scattering. As a result, they can be represented by numbers, I_{Dtol} and I_{PDMS} and, for a given polymer volume fraction ϕ, the incoherent part of the signal, $I_{inc}(\phi)$, can be approximated by $\phi I_{PDMS} + (1 - \phi)I_{Dtol}$. Note that $I_{inc}(\phi)$ varies strongly with ϕ because the incoherent scattering of protons, essentially contained in the PDMS background sample, is much larger than that of deuterons, essentially contained in the solvent. In practice we found $I_{PDMS} \approx 0.835$ cm^{-1} and $I_{Dtol} \approx 6.77\ 10^{-2}$ cm^{-1}. The relative uncertainty on I_{Dtol} is much larger than that on I_{PDMS}. Presumably, it arises from the variable remaining proton contents of the solvent (we used different trade marks for the deuterated toluene). For each series of experiment, we measured I_{PDMS} and I_{Dtol} and determined the $I_{inc}(\phi)$ interpolation formula. The calculated values $I_{inc}(\phi)$ were subtracted from $I_t(q)$ to obtain the coherent scattering cross section per unit volume.

Light Scattering. The light scattering setup comprises an argon laser source ($\lambda = 4880$ Å), a homemade goniometer, a photomultiplier, a photon counting device, and a correlator (ALV 5000). The measuring cell, a tube or a disk, is immersed in a toluene bath with temperature control. A stepping motor allows us to translate the scattering cell so that various scattering volumes can be probed. The image of the scattering volume is formed onto the surface of the detector by means of a lens (focal length f) placed in between the scattering volume and the photomultiplier at a distance $2f$ of each. The number of coherence areas can be varied by adjusting the size of two pinholes located on each side of the lens. Two different types of scattering geometries have been used.

In the first one, the sizes of the pinholes are rather large (350 μm and 1 mm). Thus the effective scattering volume is large and many coherence areas are collected at the same time by the sensitive area of the detector: the scattering device measures, by construction, a time and an "ensemble-averaged" scattered intensity $\langle I_i(\mathbf{q})\rangle_E$, analogous to the one measured in neutron scattering experiments.

In the second scattering geometry, the sizes of the apertures in front of the photomultiplier are much smaller (100 and 350 μm), and the detection is performed on one single coherence area. Under such conditions, the intensity measurement which is made does not correspond anymore to an ensemble average. In order to get an ensemble averaged intensity, it is then necessary to average the intensities recorded for many sample positions. This can be achieved, under the assumption of statistical translational invariance of the speckle pattern, with a method[9,10] that consists of moving the sample, keeping the position of the detector fixed. This method permits us to separate the respective contributions of the scattered intensities associated with static and thermal fluctuations of concentration.

The coherence factor $\beta \approx n^{-1/2}$ of the scattering geometry is readily obtained from the amplitude $1 + \beta^2$ of the ICF (eq 12) measured on a dilute solution of latices. In this study we used n values between 1 and 2, depending on the purpose of the measurements.

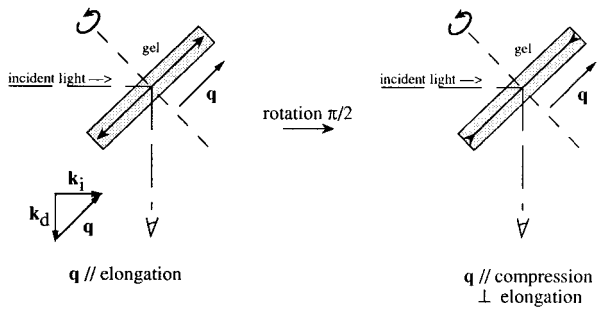

Figure 2. Sketch of the geometry used for light scattering experiments on anisotropically swollen gels. The translation of the samples is performed along the direction perpendicular to the plane containing $\mathbf{k}_i$ and $\mathbf{k}_d$.

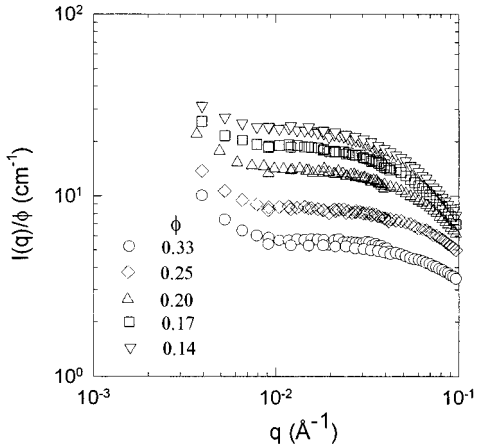

Figure 3. Absolute scattering intensities (in cm^{-1}) divided by polymer volume fraction for a series of entangled solutions of a PDMS "gum" ($M_n \approx 2.7 \times 10^5$, $M_w/M_n = 3.0$) with different concentrations.

In practice, the scanning of the gel in the laser beam is simply guided by an upper plastic support, in the case of cylindrical samples in glass tubes. In the case of the anisotropic sample, the cell, a disk, is fitted to a metal frame which is moved vertically along two rails. The frame is oriented parallel to the vector $\mathbf{q}$ (see Figure 2). The elongation axis of the sample can be oriented either horizontally or vertically, by rotation of the cylindrical cell in the frame, therefore corresponding respectively to the probe of a $\mathbf{q}$ vector parallel or perpendicular to the elongation axis, which is the minor axis of the ellipse before swelling.

For both isotropic or anisotropic samples, the cell is immersed in the toluene bath and a few thousand positions of scattering volumes, spanning a few millimeters in the gel, have been probed, twice each, in a back and forth movement. The measuring time for each position was 10 s.

To achieve an elongation in the scanning light scattering experiments the method of anisotropic swelling was preferred to mechanical elongation because it allows for a perfect stability. When the samples were stretched by their extremities, we indeed observed some drift of the ensemble-averaged intensity (on subsets) during the 16 h necessary for a scan over 4000 positions. In this case, the sample may swell under stretching (as it is immersed in a solvent reservoir) and is also liable to slip within the clamps.

IV. Results

Static Neutron and Light Scattering from Solutions. We consider first the semidilute or concentrated solutions of poly(dimethylsiloxane) in toluene, which we would like to take as reference systems for dealing with the fluctuations of polymer concentration in our gels.

In Figure 3, we reported the absolute scattering intensity $I(q)$ normalized by the polymer volume fraction ϕ, for $0.143 < \phi < 0.33$, the polymer being the "gum". The curves level off at small q values and decay at larger ones, with a position of the crossover which is shifted to the larger q as ϕ is increased. In this representation, the scattering curves meet at large q values, for $\phi < 0.25$. However, the superposition of the intensities is no longer obtained for the larger concentrations ($\phi > 0.25$), because, presumably, it would happen only at the right of the spectrometer window, at even larger q values.

Such behaviors are consistent with the predictions of the scaling theory of semidilute solutions in a good solvent[2] from which we expect

$$I(q) \sim \frac{\phi^2 \xi^3}{1 + q^2 \xi^2} \quad q\xi < 1$$
$$\xi \sim \phi^{-\nu/(3\nu-1)} \qquad (23)$$
$$\nu \approx 0.588$$

For very small q values, an upturn not predicted by the scaling theory can be observed. A comparable phenomenon, known as the Picot−Benoît effect[33] is observed, in the same q-range, at even smaller concentrations, in semidilute solutions of polystyrene. This effect is likely to originate in interchain associations (or even knots), but at the moment, no interpretation lies beyond controversy. In the present case, since these solutions were not filtered, the responsibility of the dust cannot be ruled out with entire confidence. However, no upturn was visible for unfiltered solutions made of polymer with lower molecular weights (the "oil"). Therefore, it is very likely that the so-called Picot−Benoît effect also exists in the case of PDMS.

The data can be analyzed quantitatively by using the Ornstein−Zernike plot, i.e. by plotting $I^{-1}(q)$ vs q^2 for the data points that start to level off at low q values, forgetting those corresponding to the very low q upturn. The values of ξ and $I(0)$ which are obtained this way can be fitted approximately to scaling laws, and one finds $\xi \sim \phi^{-0.8}$ and $I(0) \sim \phi^{-0.95\pm0.05}$. The variation of ξ with ϕ is not too far from that predicted for semidilute solutions (eq 23), but the experimental variation for $I(0)$ is significantly different from the one in eq 23.

One possible explanation for the larger than expected value of this exponent could arise from the fact than one probes here the polymer−polymer correlations in a concentration range that no longer corresponds to the semidilute regime but rather to the concentrated regime. In this regime, the mean curvilinear distance between interchain contacts becomes rather short and the intrinsic rigidity of the chain becomes relevant. Indeed, the excluded volume interaction of a chain with itself demands, to be effective on short distances, the existence of small loops. However the rigidity opposes the formation of such small loops. As a result, the excluded volume of the chain may not be effective on small distances and locally Gaussian statistics of the chains is expected. Then the value of the exponent ν will be close to $^1/_2$ on short distances along the chain. Introducing this value in the numerator of eq 23 leads to a value equal to unity for the exponent of $I(0)$ as a function of ϕ.

These results are consistent with the ones obtained from light scattering experiments performed on a larger series of solutions with the conventional method, that is, with the detector spanning many coherence areas. The solutions were made either with the "gum" ($M_n \approx 2.7 \times 10^5$) for the lower concentrations or with the "oil" ($M_n \approx 7.2 \times 10^4$) for the larger ones ($\phi > 0.25$), which were filtered (see Experimental Section). In such conditions, no upturn comparable with the one visible in Figure 3 has been found. As could be guessed, the angular variation is too weak (except for the lower concentrations which have been considered) to allow the determination of a correlation length, the minimum value accessible for ξ in the light scattering experiment being on the order of 150 Å.

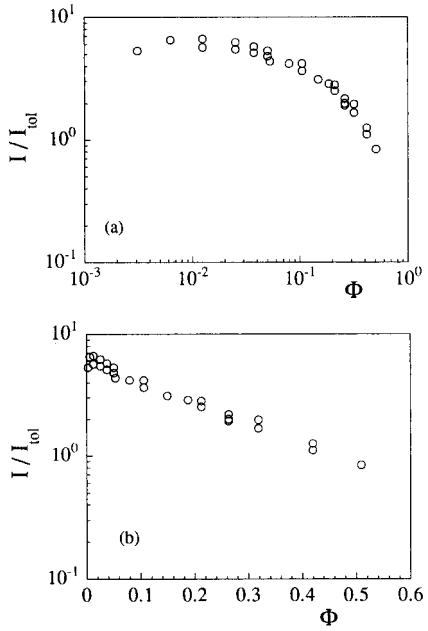

Figure 4. Light scattering intensities for PDMS solutions of various concentrations: (a) log−log scales; (b) semilogarithmic scales.

Since in these light scattering experiments, the measured intensities vary weakly with q, we show only the extrapolated intensities $I(0)$ and, in a few cases, the intensities measured at 90° ($q = 2.73 \times 10^{-3}$ Å^{-1}). The extrapolation has been performed as before, using an Ornstein−Zernike plot, which was almost flat for $\phi > 0.1$. The data are gathered in Figure 4a on a double logarithmic scale, and it can be seen that no significative difference can be detected between the true extrapolations and the measurements at 90°. The resulting curve exhibits some curvature, but the limiting behaviors, in the truly semidilute and concentrated regimes, are consistent with expectations. In Figure 4a, at low polymer concentrations, the experimental variations correspond roughly to the scaling law $I(0) \sim \phi^{-0.31}$, theoretically predicted for semidilute solutions (see above, eq 23). On the other hand, at larger polymer concentrations, there is a region where $I(0)$ decays approximately like ϕ^{-1}, which corresponds to the variation found above by neutron scattering in the same concentration range.

However, surprisingly enough, the same data points are much better aligned, almost in the whole concentration regime, on a semilogarithmic scale (see Figure 4b). More precisely, the experimental variation of $I(0)$ is consistent with the behavior $I(0) \sim \phi^{-0.31} \exp(-\phi/\phi^{**})$, with $\phi^{**} \approx 0.24$. This behavior could possibly describe the crossover in the concentrated regime for the requirement of a zero scattering intensity in the bulk conditions. In any case, this question is secondary for

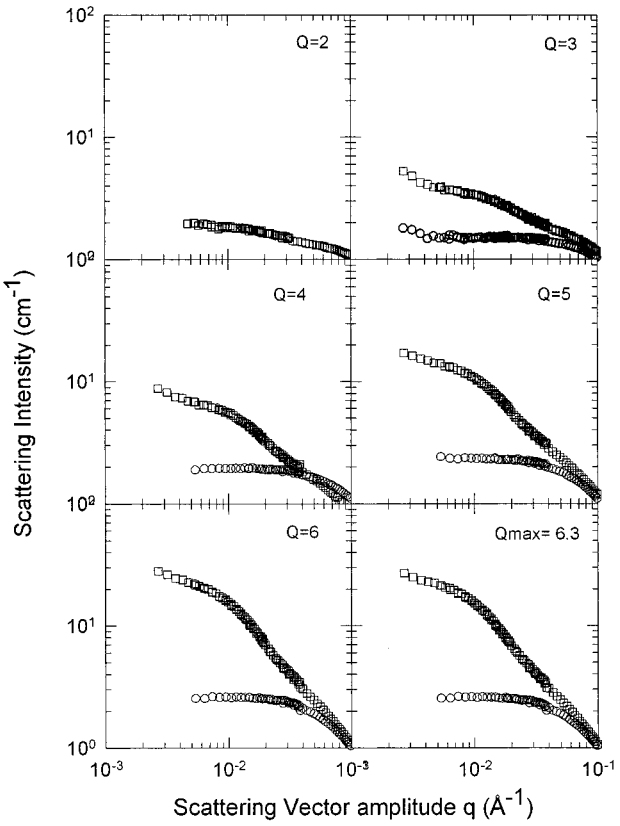

Figure 5. Scattering intensities as a function of scattering vector amplitude for a network of type 9200SiH, at different degrees of swelling Q in deuterated toluene (squares) and for entangled solutions with the same polymer volume fraction as that of the gels (circles). Spectra were obtained on two or three spectrometer (D11-ILL) configurations: 10 m, 5 m, and 1.7 m, with $\lambda = 12$ Å.

the present paper which is centered on gels. In this respect, the important conclusion of this section is that no serious contradiction is observed with respect to the standard behavior with, in particular, no upturn at very small angles and that the gels are studied in a concentration regime where the zero angle scattering intensities of the solution decay approximately like ϕ^{-1}.

Neutron Scattering from Gels. We now turn to the presentation of the scattering by the four types of PDMS gels which we have studied. Consider first, in Figure 5, the scattering intensity of sample 9200SiH at several swelling degrees Q, ranging in between $Q = 2$ and $Q = 6.3 \pm 0.25$ (maximum swelling). For each Q value, we also plotted the scattering intensity from a solution with same polymer concentration. It is readily seen that, at low q values, the scattering intensity from the gels is larger than that of the comparable solutions and that the difference increases significantly with Q. Note that it is not only the excess of intensity which is enhanced but also the absolute intensity, e.g., for $q < 10^{-2}$ Å^{-1}. Such a behavior is qualitatively similar to the one observed for previously studied gels,[5] which were made either by statistical cross-linking of long chains or by end-linking of short chains. At larger q values, the signals from the gel and from the solution almost exactly merge, typically for $q > 1/\xi_{sol}$ where ξ_{sol} denotes the correlation length of the comparable solution. It may therefore be inferred that, for length scales $l_s < \xi_{sol}$, the fluctuations of polymer concentration are very similar in both systems. Conversely, on the relatively large length scales such as $l_s \gg \xi_{sol}$, they are more important in the case of gels and are strongly

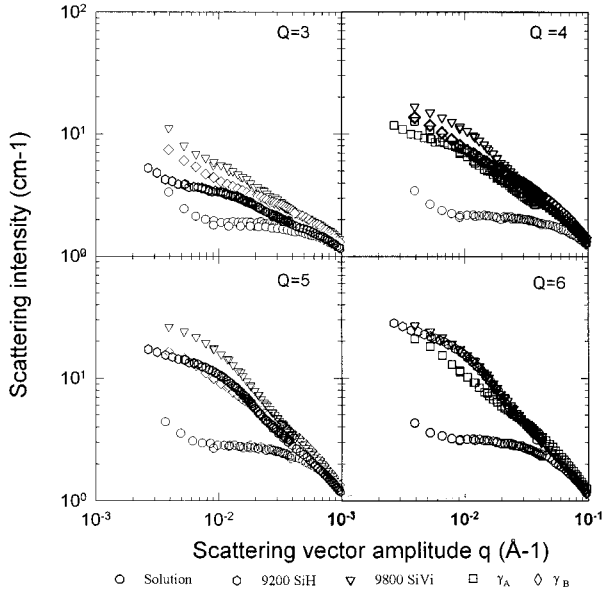

Figure 6. Scattering intensities as a function of scattering vector amplitude, at different degrees of swelling Q, for gels prepared with different methods (see Table 1) and the equivalent solutions.

amplified as the network is swollen. A first attempt at quantifying this effect consists of fitting the data at low q to an Ornstein−Zernike function, using the procedure described above for solutions. Such a method, which was used previously in the case of other networks,[34−36] is especially questionable in the present case since the shape of the scattering curves is undoubtedly more complicated than for solutions: the clear change of slope for $q \approx 5 \times 10^{-2}$ Å^{-1} indicates that the data cannot be described using a single length scale.[37−39] Moreover, there is apparently a sort of upturn at very low q values: a steeper increase is visible for the first points of the spectra in Figure 5.

Let us look now at the other PDMS gels. As can be seen in Figure 6, the scattering functions do not differ strongly from each other. Despite the difference of elastic modulus in bulk, the other end-linked network (9800SiVi) exhibit a structure factor which is almost identical, for all swelling degrees, to that of the complementary system (9200SiH). The structure factors corresponding to the statistically cross-linked networks are also similar to each other, again despite their difference of modulus in bulk (a difference which is smaller than before). The shape of the scattering envelope does not look the same for both types of cross-linking methods and seems to be more complicated in the case of the γ-irradiated systems. However, altogether, the differences of absolute intensity in between the four spectra, for a given swelling degree Q or scattering vector amplitude q, remain small. This is a bit surprising: the spatial fluctuations of polymer concentration seem therefore to be weakly correlated to the efficiency of the cross-linking reaction and not as much to the cross-linking method.

The scattering from the irradiated sample γ_A (see Table 1), submitted to uniaxial deformations, has also been studied. The sample was mechanically stretched by its extremities in an airtight container, made of stainless steel, the neutron beam and the small angle scattering signal passing through two quartz windows. The swelling ratio Q of the gel was roughly equal to 6.5 (a few drops of solvent were added in the container in order to reduce the deswelling). The results obtained

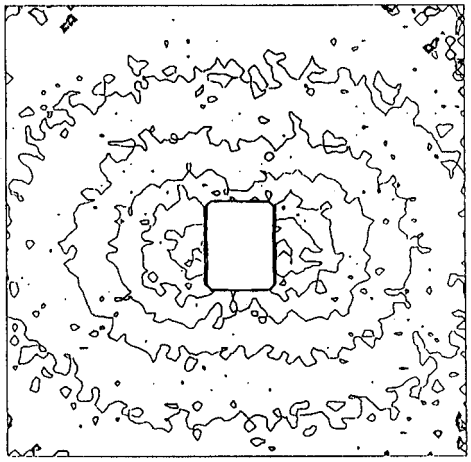

Figure 7. Isointensity contour plot of the intensity scattered from gel γ_A ($Q \approx 6.5$), mechanically stretched by a factor $\alpha = 1.3$ (the stretching direction is horizontal). The q values span the range 4×10^{-3} to 2.5×10^{-2} Å^{-1}.

for an extension ratio $\alpha = 1.3$ are presented in Figure 7. It can be seen in Figure 7 that the isointensity lines have the shape of double-winged curves with a major axis aligned with the stretching direction ("butterfly patterns"[40]). The orientation of these patterns, opposite to the one predicted by the classical theory of thermal fluctuations, arises essentially from the strong increase of scattering intensity, for **q** parallel to the stretching axis. A true mechanical stretching is not necessary to observe such an effect. The anisotropic swelling procedure, described in the experimental section, which may be compared to an elongation by a factor $\alpha = 1.59$, indeed leads to a similar behavior.[14]

To summarize this section, the scattering behaviors of several types of PDMS gels show that the spatial fluctuations of polymer concentration with wavevectors $q < 1/\xi_{sol}$ are amplified either isotropically upon a raise of the swelling ratio or anisotropically (along the direction of extension) upon an uniaxial deformation. Such phenomena seem to be quite universal since the present observations for PDMS gels, prepared here in the bulk using three different methods (see also Geissler et al.[16,37,41]), are qualitatively similar to those previously made for several types of polystyrene,[35,36,42,43] poly(vinyl acetate),[38,39,44,45] poly(vinyl alcohol),[46] or polyacrylamide[47] gels synthesized in the presence of solvent (for a review, see ref 5). We are therefore not facing a feature characteristic of a very special molecular architecture. In this context, the next step is clearly to measure the respective contributions of the thermal and quenched fluctuations to this enhancement. We address this question in the next section.

Static and Dynamic Light Scattering from Gels. Static Scanning Measurements. As was recalled in section II, time-averaged scanning measurements on a single coherence area provide a way to separate the thermal and quenched parts of the scattering intensity. We first used this method to analyze the effect of a change of swelling degree Q on two samples of type 9200SiH. In Figure 8 are shown the scanning measurements for a solution and for the gels at swelling degrees $Q = 2$, 4, 3.25, 3.9, 5 and 6 (Q_{max}), the intensity being recorded at $\theta = 90°$. It is readily seen that the increase with Q of the ensemble-averaged intensity arises mostly from an enhancement of the part of the intensity that varies with the position of the scattering volume and that is associated with quenched fluctuations.

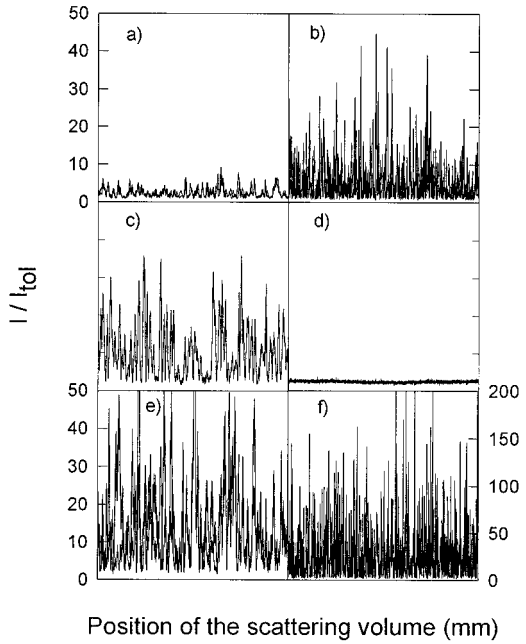

Figure 8. Scanning measurements of the scattering intensity for gel 9200SiH with different swelling degrees and for a solution measured with the same set-up. All scannings are back and forth at $\theta = 90°$. Key: (a) $Q = 2.4$, scanning of 3000 points over 10 mm; (b) $Q = 3.25$, scanning of 4000 points over 8 mm; (c) $Q = 3.9$, scanning of 4000 points over 10 mm; (d) solution equivalent to (c) ($\phi = 0.256$), scanning of 2000 points over 10 mm; (e) $Q = 5$, scanning of 4000 points over 10 mm; (f) $Q = 6$, scanning of 4000 points over 6 mm. The method of preparation for all the gels is the same although they do not come necessarily from the same batch: (a and e) made in tubes of 6 mm bore; (b and f) made in tubes of 12 mm bore; (c) made in the form of a slab (same batch as for the anisotropically swollen sample). Note that the vertical scale for part f is multiplied by a factor of 4.

Table 2. Variation with Swelling Degree Q of the Frozen Intensity I_c, of the Fluctuating Intensity I_f for the Gel 9200SiH (see Table 1), and of the Corresponding Intensity I_{sol} Scattered from the Equivalent Solution[a]

Q	I_c	I_f	I_{sol}
2.4	1.3	1.2	1.1
3.25	5.1	1	1.8
3.9	7	2.4	2
5	11.5	2.2	2.5
6	37	2.5	2.8

[a] Scattering intensities are normalized by the scattering intensity of the toluene solvent in the same conditions ($\theta = 90°$, $n \approx 1$).

The distributions of intensities corresponding to these data have been analyzed and an exponential decay with a cutoff at low I_i values is found in all cases, in good agreement with eq 10. The values obtained at different swelling degrees for I_f and for I_c (for $q = 2.73 \times 10^{-3}$ Å^{-1}) are gathered in Table 2, together with the values I_{sol} measured, with the same setup, for entangled solutions of same concentration as that of the gels.

In Table 2 the values measured for I_{sol} are nearly equal to those found for I_f within experimental accuracy, which is about 30% for these quantities. In this case, experimental errors arise in particular from the fact that the number of photon counts becomes closer to the electronic noise for these small intensities values, when they are measured on one single coherence area. It can be noticed that the intensity of the incident beam cannot be increased too much since thermal lens effects then begin to appear. Therefore we cannot conclude whether I_f is slightly depressed with respect to I_{sol}, as predicted

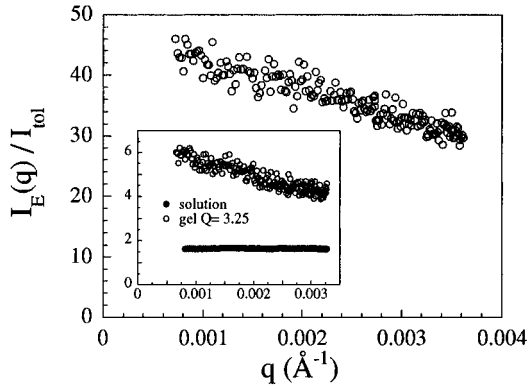

Figure 9. Ensemble-averaged intensity $I_E(q)$ scattered from gel 9200SiH swollen at equilibrium. The ensemble average is obtained by measuring the signal on a large number of coherence areas ($n \approx 100$). The insert shows the same quantities for the same gel swollen at $Q = 3.25$ and the corresponding solution.

by the classical picture,[7] or, on the contrary, slighly enhanced, as was found by Horkay et al.,[45] using another technique, or by Joosten et al.,[10] using the same one. As a consequence of the similar values of I_{sol} and I_f, the latter can be as well described by a ϕ^{-1} law in the range of polymer concentration investigated here.

On the other hand, it is clear that, as the swelling degree increases, the enhancement of the quenched part of the intensity is much stronger and accounts for most of the raise of the ensemble-averaged intensity. For the sake of comparison, the quenched part of the intensity is found to vary with the polymer concentration as $I_c \sim \phi^{-3.3\pm0.3}$. However we can note already that the question arises whether the average macroscopic concentration is the good variable that governs the increase of the quenched intensity. This point will be discussed later on.

We did not perform this type of analysis for different scattering angles because it would have cost too much time: in the case of a detection on one coherence area, the calculation of an ensemble-averaged intensity value becomes meaningful only when a few thousand scattering volumes have been probed. However we checked for the angular dependence of the average scattering intensity measured on a large number of coherence areas ($n > 100$), which is equivalent to an ensemble-averaged intensity. The intensity profile was found to be weakly dependent on the scattering wavevector (Figure 9) which indicates the absence of any characteristic length larger than about 300 Å. Considering the weak q dependence of I_{sol} in this range of polymer concentration and q values, this means that I_c is as well weakly dependent on q under the same conditions, if the equality $I_f \approx I_{sol}$ holds in the whole q range.

In order to test the effect of an uniaxial deformation on the quenched and thermal parts of the scattering intensity, we performed some light scanning experiments on the anisotropically swollen sample which exhibits "butterfly patterns" (see above and ref 14). Deuterated toluene was simply replaced by regular toluene in the same measuring cell.

For the two configurations defined by the elongation and the orientation of the sample, we observed, as before, variations of the scattering intensity with the position of the sample, but with very different amplitudes. As can be seen in Figure 10, the ensemble-averaged intensity and the amplitude of the positional fluctuations are much larger in the parallel direction

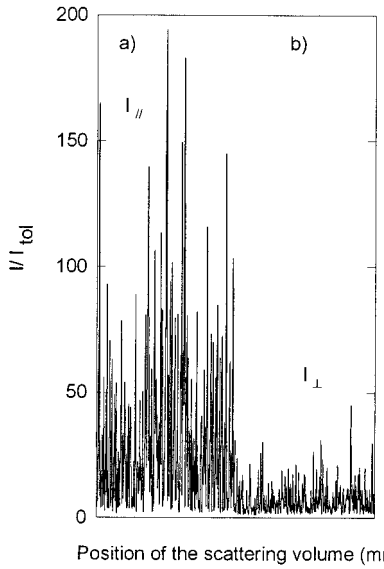

Figure 10. Scanning measurements of the intensities scattered in the directions parallel (a) and perpendicular (b) to the elongation for gel 9200SiH swollen at equilibrium.

Table 3. Variation with the Direction of Scattering Wavevector of the Frozen Intensity I_c and of the Fluctuating Intensity I_f, for the Gel 9200SiH (see Table 1), and of the Corresponding Intensity I_{sol} Scattered from the Equivalent Solution[a]

direction	I_c	I_f	I_{sol}
$\|\|$	30	2.4	2
$\perp$	5.5	2.2	2

[a] Scattering intensities are normalized by the scattering intensity of the toluene solvent in the same conditions ($\theta = 90°$, $n \approx 1$).

than in the perpendicular one. The distribution of intensities have been analyzed in all the studied configurations and as before could be fitted to eq 10. The corresponding values for I_f and for I_c are listed in Table 3. It is clear that I_f is not affected by the deformation and remains equal, within a very good approximation, to the intensity I_{sol} scattered from an equivalent solution. The anisotropic enhancement of the ensemble-averaged intensity upon the deformation is therefore entirely governed, within experimental accuracy, by the frozen-in intensity I_c.

It can be concluded from this section that, upon an isotropic or an anisotropic deformation of the gels, the part of the intensity associated with the thermal fluctuations remains very comparable to that of an entangled solution with the same polymer concentration. Thus the amplification of the ensemble-averaged intensity with swelling degree and all the anisotropic changes corresponding to the butterfly patterns arise from the variation of the quenched part of the intensity.

Dynamic Scanning Measurements. As shown in section II and in the Appendix, the dynamics of the thermal fluctuations in gels can be characterized in a meaningful way only by calculating the ensemble-averaged dynamic structure factor $f_E(\mathbf{q},t)$ from the ensemble-averaged ICF $g_E^{(2)}(\mathbf{q},t)$, measured for a large set of sample positions in a scanning experiment. As a direct consequence of the quenched fluctuations acting as local oscillators and creating the conditions for a partially heterodyned detection of the field scattered by the thermal fluctuations, $f_E(\mathbf{q},t)$ does not decay to 0 at large times and levels off to a finite value $f_E(\mathbf{q},\infty)$. The time-averaged ICF $g_i^{(2)}(\mathbf{q},t)$ measured from each scattering volume are given by eq 13, and the implications

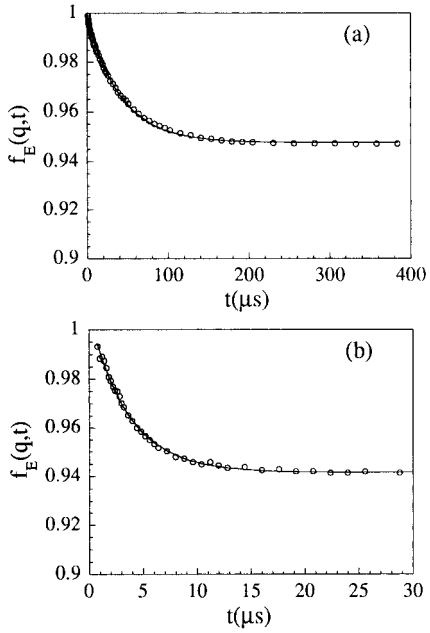

Figure 11. Ensemble-averaged dynamic structure factors measured on gel 9200SiH for two scattering angles: (a) $\theta = 30°$, $q = 10^{-3}$ Å^{-1}; (b) $\theta = 150°$, $q = 3.73 \times 10^{-3}$ Å^{-1}. The continuous lines are the fits by eq A13 with a single exponential decay for $g_f^{(1)}(t)$.

for their amplitude and their decay time can be easily checked.

As an example, we show some of the results obtained with the gel 9200SiH at maximum swelling. The measurements were performed over a set of 600 scattering volume positions, with an aperture equal to the size of a coherence area. To build each correlation function, the intensity was recorded during times ranging between 100 and 500 s. The scattering angles were ranging in between 15 and 150°. From $g_E^{(2)}(\mathbf{q},t)$ we calculated the ensemble-averaged dynamic structure factor $f_E(\mathbf{q},t)$ (see eq. (A12)). The results obtained for the scattering angles 30 and 150° are displayed in Figure 11. Before proceeding further with the ensemble-averaged dynamic structure factor, it is interesting to have a closer look at the time-averaged $g_i^{(2)}(\mathbf{q},t)$.

According to eq 13, the amplitude $g_i^{(2)}(\mathbf{q},0)$ is directly given by the strength of the local oscillator and a plot of $[g_i^{(2)}(\mathbf{q},0) - 1]\ I_i^2(\mathbf{q})$ vs $I_i(\mathbf{q})$ should yield a straight line[15,48] with a slope equal to $2I_f(\mathbf{q})$ and an intercept at the origin equal to $-I_f(\mathbf{q})$ ($I_f(\mathbf{q}) + 2I_s$) if the intensity I_s scattered from the solvent is taken into account (see Appendix). This representation is shown in Figure 12, and a good agreement with the expected linear behavior is observed. This agreement confirms that $I_f(\mathbf{q})$ is independent of the scattering volume and, moreover, that the heterodyning efficiency keeps a constant value, independent of the scattering volume, when the detection is performed over one coherence area. The latter result does not hold true as soon as n becomes larger than 1, and in the representation of Figure 12, the experimental points then fill the whole area under the line given by eq 13. The analysis in Figure 12 provides an other independent measurement of $I_f(\mathbf{q})$ that can be compared to the value measured from the histogram of $P(I_i(\mathbf{q}))$ (eq 10).

Concerning the time dependence of the ICF, if we assume a single exponential decay with a decay time τ_f for $g_f^{(1)}(\mathbf{q},t)$, then $g_i^{(2)}(\mathbf{q},t)$ as given by eq 13 is the sum of

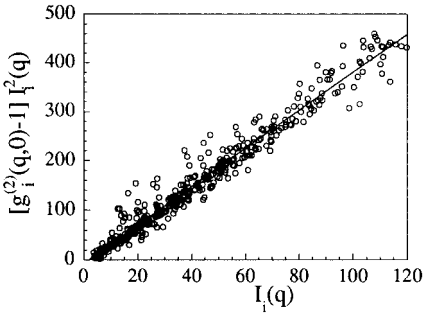

Figure 12. Plot of the quantity $[g_i^{(2)}(\mathbf{q},0) - 1]I_i^2(\mathbf{q})$ vs $I_i(\mathbf{q})$ for the autocorrelation functions of the intensity $g_i^{(2)}(\mathbf{q},t)$ measured on 600 different scattering volumes. According to eqs 13 and A6 the slope of the linear fit yields $2I_f(\mathbf{q})$. The sample is gel 9200SiH swollen at equilibrium ($\theta = 30°$). Intensities are normalized by the intensity scattered from toluene.

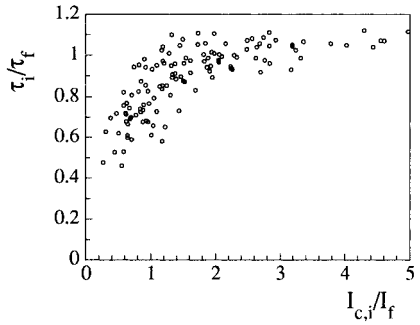

Figure 13. Evolution of the relaxation time τ_i determined from $g_i^{(2)}(\mathbf{t})$ with the ratio $I_{c,i}/I_f$ during a scan through different scattering volumes. The sample is gel 9200SiH swollen anisotropically (see Experimental Section), and the data correspond to the experimental geometry where $\mathbf{q}$ is perpendicular to the direction of elongation.

two exponentials. Depending on the ratio $I_{c,i}/I_f$, one expects two clear limits.[48,49]

(i) The first is the homodyne limit, when $I_{c,i}/I_f \ll 1$, for which $[g_i^{(2)}(\mathbf{q},t) - 1]$ exhibits an apparent decay time essentially equal to $\tau_f/2$. In other words, the effect of the frozen-in fluctuations is negligible in this case.

(ii) The second is the heterodyne limit, when $I_{c,i}/I_f \gg 1$, for which $[g_i^{(2)}(\mathbf{q},t) - 1]$ exhibits an apparent decay time essentially equal to τ_f. The second term in the right hand side of eq 13 is then dominating the decay of the ICF.

In the intermediate situations, the factor of 2 in the decay times of the two exponentials is too small to allow their separation and to estimate their respective amplitudes. But, on the other hand, the fact that we have only a factor of 2 allows a rather satisfactory fit by a single exponential, decaying with an apparent time τ_i such that $\tau_f/2 < \tau_i < \tau_f$. Thus, τ_i should vary in between the homodyne limit $\tau_f/2$ and the heterodyne limit τ_f as the ratio $I_{c,i}/I_f$ is increased. As can be seen in Figure 13, the agreement is very satisfactory: τ_i increases almost exactly by a factor of 2 as $I_i(\mathbf{q})$ is increased. This confirms the existence of a single relaxation time τ_f that is independent of the scattering volume and that characterizes the thermal fluctuations of polymer concentration. Once again, if the detection is performed with a value of n larger than 1, the data points do no longer follow a master curve but fill the whole area under that curve. This corresponds to an heterodyning efficiency that depends on the scattering volume.

The behaviors reported in Figures 12 and 13 indicate that everything happens as if our gel was consisting of

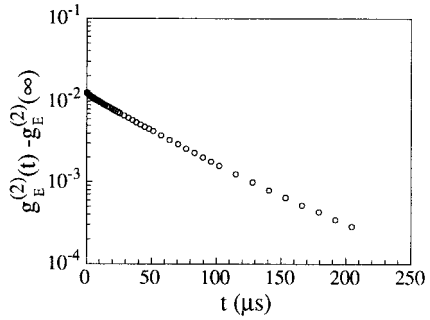

Figure 14. Ensemble-averaged intensity correlation function measured at $\theta = 30°$ with a large number of coherence areas ($n \approx 100$). The sample is gel 9200SiH swollen at equilibrium.

Table 4. Analysis of the Correlation Functions for Sample 9200SiH Swollen at Equilibrium[d]

θ	q (10^{-3} Å^{-1})	$\tau_f{}^a$ (μs)	$\tau_f{}^b$ (μs)	$\tau_f{}^c$ (μs)
15	0.504	175		
30	1.00	47	42	53
90	2.73	6.1		
150	3.73	3.5	3.6	

[a] From the excursion of τ_i values. [b] From the ensemble-averaged dynamic structure factor ($n = 1$). [c] From the ensemble-averaged dynamic structure factor measured on a large number of coherence areas ($n \approx 100$). [d] From the characteristic times, the following values of the cooperative diffusion coefficient (in cm^2/s) can be calculated: 2.2×10^{-6} (*a*); 2.2×10^{-6} (*b*); 1.9×10^{-6} (*c*). These compare very well with the value $D_e = (2.2 \pm 0.2) \times 10^{-6}$ cm^2/s measured in the kinetics of swelling experiment.

a fairly homogeneous fluctuating medium in which frozen-in scatterers were dispersed, acting as local oscillators for the quasi-elastic light scattering experiment. Thus a collective diffusion constant D_c can be calculated as $D_c = (\tau_f q^2)^{-1}$ where τ_f is determined from the excursion of the values of τ_i.

However, back to the ensemble-averaged dynamic structure factor, it is more straightforward to determine τ_f by analyzing $f_E(\mathbf{q},t)$ according to eq A13. The corresponding fitting curves are shown in Figure 11.

Finally it is worth mentioning that, once the validity of the above description is well established by measurements on one coherence area, from the experimental point of view it is easier to measure directly an ensemble-averaged dynamic structure factor with a configuration of detection corresponding to a large number of coherence areas ($n \approx 100$). In this case, the ensemble-averaged dynamic structure factor decays to zero; i.e., the information about the ratio $I_f(\mathbf{q})/I_c(\mathbf{q})$ is lost, and the signal to noise ratio is small (Figure 14). It is difficult to calculate this ratio that depends on the mixing of the heterodyning static intensities from the different coherence areas. Nevertheless, we expect the corresponding τ_f value to be rather close to the values obtained by the two other methods. We note that, in this method, the heterodyne value of the characteristic time, i.e., τ_f, is directly measured.

Indeed Table 4 shows that the values of τ_f obtained by the three methods are in good agreement. Furthermore the corresponding values for D_c compare very well with the one obtained from the kinetics of swelling experiment.[30,49,50]

V. Discussion and Conclusion

Pusey and Van Megen[9] were the first to propose the probing of many different scattering volumes to separate the thermal and quenched fluctuations of concentration in a partly quenched medium. Their method was then applied to the study of polyacrylamide gels by Joosten and co-workers.[10] In both papers the origin of the quenched fluctuations in gels was attributed to the topological constraints in the network that limit the motion of the elementary scatterers, located at random in the medium. In this picture, if the mean-squared displacement of the scatterers is $\langle\delta^2\rangle$, the expression for the ensemble-averaged dynamic structure factor reads

$$f_E(\mathbf{q},t) = \exp\left\{-q^2\langle\delta^2\rangle\left[1 - \exp\left(-\frac{D_0 t}{\langle\delta^2\rangle}\right)\right]\right\} \quad (24)$$

D_0 being the diffusion coefficient of the scatterers in the short time limit, i.e., when they do not feel the constraints. In this approach the asymptotic limit at infinite time of $f_E(\mathbf{q},t)$ provides a measurement of $\langle\delta^2\rangle$

$$f_E(\mathbf{q},\infty) = \exp(-q^2\langle\delta^2\rangle) \quad (25)$$

if the length scale q^{-1} probed in the experiments is comparable to $\langle\delta^2\rangle^{1/2}$. On the other hand, when that length scale is much smaller than $\langle\delta^2\rangle^{1/2}$, i.e. $q^2\langle\delta^2\rangle \gg 1$, the effect of the topological constraints cannot be observed. In the opposite limit, i.e. $q^2\langle\delta^2\rangle \ll 1$, the asymptotic value $f_E(\mathbf{q},\infty)$ approaches 1, which means that the medium appears on that length scale as completely frozen, the initial decay of the dynamic structure factor being inaccessible within the experimental accuracy.[9−11]

In the gel swollen at equilibrium studied here, the very small sensitivity of the asymptotic value $f_E(\mathbf{q},\infty)$ to a variation of the scattering wavevector (see Figure 11) allows one to definitively rule out the model of scatterers with restricted motion as a possible explanation for the frozen scattering intensity: in the examples shown in Figure 11, $f_E(\mathbf{q},\infty)$ would have been expected to vary by a factor close to 14, according to eq 25. Instead, the interpretation of $f_E(\mathbf{q},\infty)$ in terms of frozen fluctuations of concentration acting as local oscillators for the dynamic light scattering experiments is fully consistent with the nearly constant value of $f_E(\mathbf{q},\infty)$ in Figure11, since then $f_E(\mathbf{q},\infty)$ is given by (see eq A13)

$$f_E(\mathbf{q},\infty) = \frac{I_c(\mathbf{q})}{I_f(\mathbf{q}) + I_c(\mathbf{q})} \quad (26)$$

which is expected to depend weakly on q from the results in Figure 9. The same conclusion was reached by Xue et al.[11] in the case of polyacrylamide gels studied in their reaction bath and by Skouri et al.[48,49] in the case of poly(acrylic acid) gels studied at varying swelling ratios.

Interestingly, our results and the discussion above show that the ensemble-averaged dynamic structure factor has to be analyzed in terms of eq A13 and that the mechanism governing the relaxation of the thermal fluctuations of polymer concentration remains the cooperative diffusion of the chains where all the chains in the network diffuse while interacting together, like in a semidilute solution.[2] In particular, a diffusion coefficient like D_0 in eq 24 would get a meaning only in the case where the fluctuations of concentration associated to a few labeled subchains of size ξ could be measured.

We now turn to the discussion of static fluctuations of concentration. They are a signature of the presence of permanent cross-links that introduce topological constraints and restrict the available configurations of

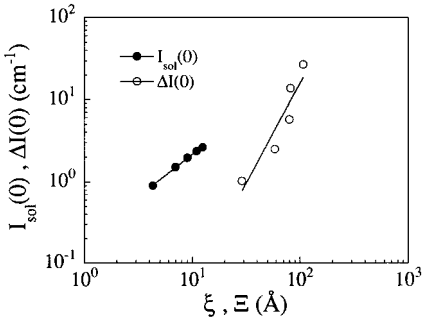

Figure 15. Variations of the intensity $I_f(q \to 0)$ scattered from the solutions and of the difference $\Delta I(q \to 0) = I_{gel}(q \to 0) - I_{sol}(q \to 0)$ as functions of the associated characteristic lengths ξ and Ξ. These quantities are determined from an Orstein−Zernike analysis of the data shown in Figure 5 (see text).

the chains in the network, compared to the ones that can be realized in a semidilute solution with same concentration.

Some time ago, it was remarked[51,52] that the statistical cross-linking of long interpenetrating chains should yield large fluctuations in the density of cross-links for gels prepared well above the gel point but still well below the cross-linking density that allows no further swelling in an excess of solvent (syneresis threshold). Such gels in their reaction bath should comprise interpenetrating zones that are more or less cross-linked, i.e., more or less rigid. In analogy with a percolation process, a fractal nature of the densely cross-linked regions would be expected. Upon swelling of the gels, such more rigid zones should swell to a smaller extent than the less densely cross-linked regions and should desinterpenetrate as the macroscopic swelling proceeds. The resulting fluctuations of concentration revealed by the swelling should then give a significant increase in the scattering intensity.

Experiments performed on polystyrene gels prepared by Friedel−Crafts random cross-linking of long chains yielded results that were consistent with the predictions of this model.[34−36] However, further experiments on gels obtained by various end-linking methods have shown that the nature of frozen concentration heterogeneities seems to depend strongly on the functionality of the cross-links and on the fluctuations of this functionality.[5] More generally it seems linked to the method of synthesis and to the conditions in the reaction bath.

In line with the idea of frozen concentration heterogeneities, it might seem natural to split the total scattering intensity into its fluctuating and quenched contributions[44] and to identify the latter to the contribution of network heterogeneities. It is worth noticing that this analysis implicitly distinguishes two components in the gel: the fluctuating solution-like part and the frozen heterogeneities. This distinction raises then naturally the question of the corresponding concentrations of these two components.[44] Without knowing these parameters, it is difficult in the frame of a two components picture to extract useful information from the variation of the frozen intensity with total polymer volume fraction. This difficulty can be avoided if we are able to deduce by an Orstein−Zernike analysis the limiting value at $q = 0$ and the characteristic length Ξ associated with the frozen intensity. This can be done for the small angle neutron scattering data in Figure 5, if we neglect the first data points at small q values and if we subtract the intensity scattered from the equivalent solutions as an approximation for the fluctuating contribution. As shown above, this approximation is very good in the q range probed by the light scattering technique. The results are displayed in Figure 15, together with the values of $I_f(0)$ and ξ obtained for the solutions. They show clearly that, for a given polymer volume fraction, the characteristic length associated to frozen heterogeneities is about one order of magnitude larger than the one associated to the thermal fluctuations. Also the variation of $I_c(0)$ vs Ξ is much steeper than the variation of $I_f(0)$ vs ξ. A power law analysis in this restricted range of variation gives exponent values about 2.4 and 1, respectively for the frozen and the thermal components.

In the case of polymer solutions, the scattering intensity at $q = 0$ and the correlation length ξ are simply related as[2]

$$I_f(0) \sim \xi^{2D-3} \tag{27}$$

where $D = 1/\nu$ is the fractal dimension of the chains. For the present solutions, the experimental value of D appears thus to be close to 2, in agreement with the behavior reported above for the light scattering results. Therefore, it seems that in this rather concentrated regime, the chains behave as Gaussian chains. Interestingly, for a percolation-type distribution of branched polymers in a semidilute solution, it can be shown[53,54] that relation 27 holds true, provided ξ is defined as the z-averaged radius of the blobs. Pursuing further the analogy between concentration heterogeneities and percolation clusters, we would then expect[53,54]

$$I_c(0) \sim \Xi^{2D'-3} \tag{28}$$

where D' would be the fractal dimension of concentration heterogeneities. The experimental data would thus lead to a value $D' \approx 2.7$, surprisingly higher than the fractal dimension of percolation clusters in their reaction bath, i.e., when excluded volume interactions are screened.

However, in the derivation of eq 28, it is explicitly assumed that Ξ is the screening length for excluded volume interactions; i.e., chains are swollen for length scales smaller than Ξ.[53,54] In the present case this is obviously not true, due to the concentrated regime investigated here. Moreover, even for gels swollen to a larger extent, with fully developed excluded volume interactions, there remains the more general problem that excluded volume interactions are screened through the thermal fluctuations of concentration, i.e., beyond length scales larger than $\xi \ll \Xi$. Therefore, the description of a swollen gel in terms of a two components system, frozen heterogeneities + solution-like part, might well be a tricky problem, much beyond the scope of the present paper. Thus, apart from the fact that the experimental intensity curves seem to show consistently at small q values an upturn that could invalidate an Ornstein−Zernike analysis, the main weakness of the above approach remains the improper description of the screening of excluded volume interactions in the gel.

An alternate view for a swollen gel is schematically depicted in Figure 16 that shows the profile of concentration $\phi(\mathbf{r},t)$ (see eqs 2−5). The thin fluctuating line corresponds to the local density $\phi(\mathbf{r},t)$ of scatterers in the gel, which are distributed randomly in space on length scales larger than a certain correlation distance Ξ. The concentration $\phi(\mathbf{r},t)$ fluctuates around a time-

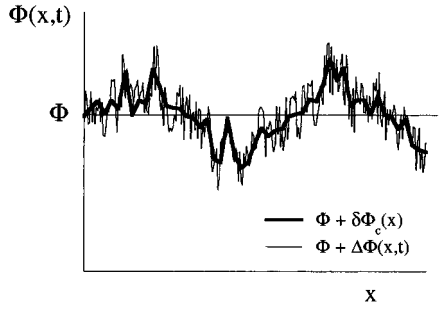

Figure 16. Schematic representation of the concentration profile in a gel along one direction. The bold line is the time-averaged profile $\Phi + \delta\Phi_c(x)$, whereas the thin line is a typical instantaneous profile $\Phi + \Delta\Phi(x,t) \equiv \Phi + \delta\Phi_c(x) + \delta\Phi_f(x,t)$ (see eqs 2−5).

averaged profile $\phi + \delta\phi_c(\mathbf{r})$ (thick line): the mountainous profile results from the frozen disorder in the spatial distribution of cross-links and/or in the connectivity of the network. In other words, thermal fluctuations of concentration are superimposed on a profile of frozen-in spatial fluctuations. In this picture, there is no attempt to distinguish two components in the gel and all scatterers contribute as well to the thermal fluctuations. The latter are governed by the cooperative diffusion of all the chains constituting the network, and they determine the screening length $\xi \ll \Xi$ for the excluded volume interactions. The frozen intensity comes from the large wavelength fluctuations of concentration that cannot relax due to the topological constraints.

Such a picture was given recently a more quantitative meaning by Panyukov and Rabin.[55,56] They were able to take into account the restriction of the available configurations introduced by the random cross-linking in the preparation state and to calculate its effects on the fluctuations of concentration after a subsequent swelling to equilibrium. In this model also, excluded volume interactions are screened out through the thermal fluctuations of the network, and the squared length Ξ^2 emerges as the coefficient of the first term in the q^2 series expansion of the inverse frozen structure factor. No fractal behavior for the frozen fluctuations is assumed and the resulting expression for Ξ has no simple variation as a function of the polymer volume fraction. Interestingly, in this model, the fluctuating intensity is not the same as the intensity scattered from an equivalent semidilute solution and includes a memory of the state of preparation. The test of this prediction lies out of the accuracy range in the present experiments. The frozen intensity in the vanishing q limit is predicted to vary as $\phi^{-7/3}$ for a gel swollen in a good solvent. This value of the exponent does not compare very well with our experimental value, which is about −3.3, but this is not very conclusive since our gels are studied in a limited range of concentration where the equivalent solutions do not exhibit a typical semidilute behavior. Moreover, a simplifying assumption made in the theory, i.e., the neglect of entanglements, bears a doubtful validity in the case of the present gels that are prepared in the melt. In addition our results concern mostly gels obtained through an end-linking reaction while in the model random cross-linking is assumed. However, in this context, it can be remarked that the general shape of the calculated structure factors compares better with the experimental ones for gels prepared by end-linking than for gels obtained by statistical cross-linking.[55,56]

To conclude, we have shown in this paper that frozen fluctuations of concentration are responsible for the excess of scattering intensity that arises in a deformed gel compared to a semidilute solution with same concentration. In a dynamic light scattering experiment, these frozen fluctuations of concentration act as local oscillators that heterodyne to a variable extent the detected signal, depending on the particular scattering volume probed. This effect can be properly taken into account by different methods that we described. The temporal decay of the ensemble-averaged dynamic structure factor is given by the thermal fluctuations of polymer concentration and is governed by the cooperative diffusion of the chains. The associated characteristic length is the screening length for excluded volume and hydrodynamic interactions in the gels. Static fluctuations of concentration are associated with a different characteristic length scale, which depends on the conditions of preparation and of study, beyond which the gels can be considered as homogeneous. The present gels are characterized by small swelling equilibrium volume ratios, and the corresponding solutions do not exhibit the typical behavior of semidilute solutions in a good solvent. Therefore, it was not possible to make a quantitative comparison with existing models for the static fluctuations of concentration. We hope that future work along the lines described in this paper will provide better conditions to test these models.

Acknowledgment. We would like to thank F. Isel for giving us access to his laboratory and for his kind assistance during the synthesis of the samples.

Appendix

In this Appendix, we derive the full expressions of the quantities introduced in section II in the special case where the intensity scattered by the solvent is considered. Thus, in the general case, we write the electric field $E_i(\mathbf{q},t)$ scattered by a volume V_i as the superposition of three scattered fields pertaining to the static fluctuations of concentrations $E_{c,i}(\mathbf{q},t)$, to the thermal fluctuations of polymer concentration $E_f(\mathbf{q},t)$ and to the thermal fluctuations of solvent density $E_s(\mathbf{q},t)$

$$E_i(\mathbf{q},t) = E_{c,i}(\mathbf{q},t) + E_f(\mathbf{q},t) + E_s(\mathbf{q},t) \qquad \text{(A1)}$$

with

$$E_{c,i}(\mathbf{q},t) = E_{c,i}(\mathbf{q}) \exp[-i(\omega t + \varphi_{c,i}(\mathbf{q}))]$$

$$E_f(\mathbf{q},t) = E_f(\mathbf{q}) \exp[-i(\omega t + \varphi_f(\mathbf{q},t))] = f_f(\mathbf{q},t)E_f(\mathbf{q})e^{-i\omega t} \qquad \text{(A2)}$$

$$E_s(\mathbf{q},t) = E_s(\mathbf{q}) \exp[-i(\omega t + \varphi_s(\mathbf{q},t))] = f_s(\mathbf{q},t)E_s(\mathbf{q})e^{-i\omega t}$$

where $f_\alpha(\mathbf{q},t) \equiv \exp[-i\varphi_\alpha(\mathbf{q},t)]$ contains the nontrivial time dependence of the phase of the scattered field $E_\alpha(\mathbf{q},t)$. Note that $\varphi_{c,i}(\mathbf{q})$ is a constant (no time dependence) that depends only on the scattering volume and that the phases $\varphi_f(\mathbf{q},t)$ and $\varphi_s(\mathbf{q},t)$ are fluctuating randomly and independently with time. These conditions are a direct consequence of the splitting of the fluctuations of concentration into a quenched and a thermal part (eqs 1−5). In the q range considered here, the field scattered by the solvent can always be considered as independent of the scattering wavevector. For the sake of simplicity, we will drop the q dependence in

the two other fields and consider it as implicit in the general case. The two functions $f_\alpha(t)$ describe the temporal correlation of the two fields associated with thermal fluctuations. Thus we have

$$\begin{aligned} \langle f_\alpha(t)\rangle_T &= 0 \\ \langle |f_\alpha(t)|^2\rangle_T &= 1 \\ \langle f_f(t')f_f^*(t'+t)\rangle_T &= g_f^{(1)}(t) \\ \langle f_s(t')f_s^*(t'+t)\rangle_T &= 0 \end{aligned} \tag{A3}$$

where the last equality results from the relaxation time of the density fluctuations of the solvent being always much smaller than the delay times measured in the experiments. The instantaneous value of the scattering intensity follows from eqs A1 and A2

$$\begin{aligned} I_i(t) &= E_i(t)\, E_i^*(t) \\ &= I_{c,i} + I_f|f_f(t)|^2 + I_s|f_s(t)|^2 + \\ &+ 2[E_{c,i}(t)\, E_f^*(t) + E_{c,i}(t)\, E_s^*(t) + E_f(t)E_s^*(t)] \end{aligned} \tag{A4}$$

and its time average is readily obtained from the conditions in eq A3:

$$I_i \equiv \langle I_i(t)\rangle_T = I_{c,i} + I_f + I_s \tag{A5}$$

From eq A4, it is then possible to write the intensity−intensity correlation function. After some standard developments and simplifications,[24] it reads

$$\langle I_i(t')I_i(t'+t)\rangle_T = I_i^{\,2} + 2I_{c,i}I_f\, g_f^{(1)}(t) + I_f^{\,2}[g_f^{(1)}(t)]^2 \tag{A6}$$

Thus the ensemble averaged ICF defined in eq 16 can be written as

$$g_E^{(2)}(t) = \frac{\langle I_i^{\,2}\rangle_E + 2I_cI_f\, g_f^{(1)}(t) + I_f^{\,2}[g_f^{(1)}(t)]^2}{I_E^{\,2}} \tag{A7}$$

where

$$I_c \equiv \langle I_{c,i}\rangle_E = I_E - I_f - I_s \tag{A8}$$

It is worthwhile to examine the limiting behaviors of the quantity defined by eq A7. Using eqs A3, A5, and A8 we obtain for the zero time limit

$$g_E^{(2)}(0) = 1 + \frac{\langle I_{c,i}^{\,2}\rangle_E - I_c^{\,2} + 2I_cI_f + I_f^{\,2}}{I_E^{\,2}} \tag{A9}$$

If the distribution of quenched intensity values obeys eq 6, eq A9 can be further transformed into

$$g_E^{(2)}(0) = 2 - 2\frac{I_s}{I_E} + \left(\frac{I_s}{I_E}\right)^2 \tag{A10}$$

Thus the intensity scattered from the solvent can be responsible for a decrease of the amplitude of the ensemble average ICF from the expected value of 2 and this has to be taken into account when defining an ensemble-averaged dynamic structure factor (eq 17) that keeps the conventional normalization, i.e., $f_E(0) = 1$. Similarly, using again the statistical properties implied by eq 6, we can calculate the long time limit of eq A7 as

$$g_E^{(2)}(\infty) = 1 + \left(\frac{I_c}{I_E}\right)^2 \tag{A11}$$

Thus the frozen intensity is responsible for an asymptotical value $g_E^{(2)}(\infty)$ that is larger than one. This is equivalent to saying that the ensemble-averaged dynamic structure factor does not decay to zero. To take into account the effect of the intensity scattered from the solvent we modify slightly eq 6 and write

$$f_E(t) = \left[\frac{g_E^{(2)}(t) - 1}{g_E^{(2)}(0) - 1}\right]^{1/2} \tag{A12}$$

which can be easily simplified into

$$f_E(t) = \frac{I_c + I_f\, g_f^{(1)}(t)}{I_c + I_f} \tag{A13}$$

If we assume now a single exponential decay for $g_f^{(1)}(t)$, i.e., $g_f^{(1)}(t) = \exp(-t/\tau_f)$, this means that the only physically relevant time in the system, τ_f, can be determined by fitting the experimental $f_E(t)$ (eqs A12 and A13) as a single exponential decay with the baseline $f_E(\infty)$ as an adjusting parameter. It can be noticed that the initial slope of $f_E(t)$ would yield in this case a value τ_0 that can be markedly different from τ_f

$$\tau_0 = \frac{I_c + I_f}{I_f}\tau_f \tag{A14}$$

References and Notes

(1) Flory, P. J. *The Principles of Polymer Chemistry*; Cornell University Press: Ithaca, NY, 1953.
(2) de Gennes, P. G. *Scaling Concepts in Polymer Physics*; Cornell University Press: Ithaca, NY, 1979.
(3) Dusek, K.; Prins, W. *Adv. Polym. Sci.* **1969**, *6*, 1.
(4) Bastide, J.; Candau, S. J.; Delsanti, M. *Adv. Polym. Sci.* **1982**, *44*, 27.
(5) Bastide, J.; Candau, S. J. In *Physical Properties of Gels*; Cohen-Addad, J. P. Ed.; John Wiley & Sons: New York, 1996.
(6) Higgins, J. S.; Benoît, H. C. *Polymers and Neutron Scattering*; Oxford Series on Neutron Scattering in Condensed Matter; Clarendon Press: Oxford, England, 1994.
(7) Tanaka, T.; Hocker, L. O.; Benedek, G. B. *J. Chem. Phys.* **1973**, *59*, 5151.
(8) Silberberg, A. In *Polyelectrolyte Gels*; Harland, R. S., Prud'homme, R. K., Eds.; ACS Symposium Series 480; American Chemical Society: Washington, DC, 1992.
(9) Pusey, P. N.; Van Megen, W. *Phys. A* **1989**, *157*, 705.
(10) Joosten, J. G. H.; McCarthy, J. L.; Pusey, P. N. *Macromolecules* **1991**, *24*, 6690.
(11) Xue, J. Z.; Pine, D. J.; Milner, S. T.; Wu, X. L.; Chaikin, P. M. *Phys. Rev. A*, **1992**, *46*, 6550.
(12) Skouri, R.; Munch, J. P.; Schosseler, F.; Candau, S. J. *Europhys. Lett.* **1993**, *23*, 635.
(13) Moussaid, A.; Candau, S. J.; Joosten, J. G. H. *Macromolecules* **1994**, *27*, 2102.
(14) Rouf, C.; Bastide, J.; Pujol, J. M.; Schosseler, F.; Munch, J. P. *Phys. Rev. Lett.* **1994**, *73*, 830.
(15) Shibayama, M.; Norisuye, T.; Nomura, S. *Macromolecules* **1996**, *29*, 8746.
(16) Mallam, S.; Horkay, F.; Hecht, A. M.; Rennie, A. R.; Geissler, E. *Macromolecules* **1991**, *24*, 543.
(17) Pusey, P. N. In *Photon Correlation and Velocimetry*; Cummins, H. Z., Pike, E. R., Eds.; Plenum: New York, 1977.
(18) Arrechi, F. T. *Phys. Rev. Lett.* **1965**, *15*, 1912.
(19) Martienssen, W.; Spiller, E. *Phys. Rev.* **1966**, *145*, 285.
(20) Goodman, J. In *Laser Speckle and Related Phenomena*; Dainty, J. C., Ed.; Springer Verlag: Berlin, 1975.
(21) Mandel, L. *Proc. Phys. Soc.* **1959**, *74*, 233.
(22) Palmer, R. G. *Adv. Phys.* **1982**, *31*, 669.
(23) Sellen, D. B. *J. Polymer Sci., Polym. Phys. Ed.* **1987**, *25*, 699.

(24) Jakeman, E. In *Photon Correlation and Light Beating Spectroscopy*; Cummins, H. Z., Pike, E. R., Eds.; Plenum: New York, 1974.
(25) Siegert, A. J. F. *MIT Radiat. Lab. Rep.* **1943**, No. 465.
(26) Karstedt, US 3 775 452, 1973.
(27) Herz, J. E.; Belkebir-Mrani, A.; Rempp, P. *Eur. Polym. J.* **1973**, *9*, 1165. Chalk, A. J.; Hanod, J. F. *J. Am. Chem. Soc.* **1965**, *87*, 16.
(28) Geissler, E.; Duplessix, R.; Hecht, A. M. *Macromolecules* **1983**, *16*, 712.
(29) Treloar, L. R. G. *The Physics of Rubber Elasticity*; Clarendon Press: Oxford, England, 1975.
(30) Tanaka, T.; Fillmore, D. J. *J. Chem. Phys.* **1979**, *70*, 1214.
(31) Li, Y.; Tanaka, T. *J. Chem. Phys.* **1990**, *92*, 1365.
(32) Ragnetti, M.; Geiser, D.; Höcker, H.; Oberthür, R. C. *Makromol. Chem.* **1985**, *186*, 1701.
(33) Benoît, H.; Picot, C. *Pure Appl. Chem.* **1966**, *12*, 545.
(34) Mendes, E. Thèse, Université Louis Pasteur, Strasbourg, France, 1991.
(35) Mendes, E.; Lindner, P.; Buzier, M.; Boué, F.; Bastide, J. *Phys. Rev. Lett.* **1991**, *66*, 1595.
(36) Mendes, E.; Oeser, R.; Hayes, C.; Boué, F.; Bastide, J. *Macromolecules* **1996**, *29*, 5574.
(37) Mallam, S.; Hecht, A. M.; Geissler, E.; Pruvost, P. *J. Chem. Phys.* **1989**, *91*, 6447.
(38) Horkay, F.; Hecht, A. M.; Mallam, S.; Geissler, E.; Rennie, A. R. *Macromolecules* **1991**, *24*, 2896.
(39) Geissler, E.; Horkay, F.; Hecht, A. M. *Phys. Rev. Lett.* **1993**, *71*, 645.
(40) Oeser, R.; Picot, C.; Herz, J. in *Polymer Motions in Dense Systems*; Richter, D., Springer, T., Eds.; Springer Proceedings in Physics 29; Springer Verlag: Berlin, 1988.
(41) Hecht, A. M.; Guillermo, A.; Horkay, F.; Mallam, S.; Legrand, J. F.; Geissler, E. *Macromolecules* **1992**, *25*, 3677.
(42) Hecht, A. M.; Horkay, F.; Mallam, S.; Geissler, E. *Macromolecules* **1992**, *25*, 6915.
(43) Mendes, E.; Girard, B.; Picot, C.; Buzier, M.; Boué, F.; Bastide, J. *Macromolecules* **1993**, *26*, 6873.
(44) Hecht, A. M.; Horkay, F.; Geissler, E.; Benoit, J. P. *Macromolecules* **1991**, *24*, 4183.
(45) Horkay, F.; Burchard, W.; Hecht, A. M.; Geissler, E. *Macromolecules* **1993**, *26*, 4203.
(46) Geissler, E.; Horkay, F., Hecht, A. M. *Macromolecules* **1991**, *24*, 6006.
(47) Mallam, S.; Horkay, F.; Hecht, A. M.; Geissler, E. **1989**, *22*, 3356.
(48) Skouri, R. Thèse, Université Louis Pasteur, Strasbourg, France, 1994.
(49) Skouri, R.; Schosseler, F.; Munch, J. P.; Candau, S. J. *Macromolecules* **1995**, *28*, 197.
(50) Peters, A.; Schosseler, F.; Candau, S. J. In *Polymers in Aqueous Media: Performance Through Association*; Glass, J. E., Ed.; Advances in Chemistry Series 223; American Chemical Society: Washington, DC, 1989.
(51) Bastide, J.; Leibler, L. *Macromolecules* **1988**, *21*, 2647.
(52) Bastide, J.; Leibler, L.; Prost, J. *Macromolecules* **1990**, *23*, 1821.
(53) Daoud, M.; Leibler, L. *Macromolecules* **1988**, *21*, 1497.
(54) Munch, J. P.; Delsanti, M.; Durand, D. *Europhys. Lett.* **1992**, *18*, 577.
(55) Panyukov, S.; Rabin, Y. *Phys. Rep.* **1996**, *269*, 1.
(56) Panyukov, S.; Rabin, Y. *Macromolecules* **1996**, *29*, 7900.

MA970916Z